Commun. Comput. Phys.
doi: 10.4208/cicp.OA-2017-0041

Vol. **23**, No. 3, pp. 685-705
March 2018

An Efficient Monte Carlo-Transformed Field Expansion Method for Electromagnetic Wave Scattering by Random Rough Surfaces

Xiaobing Feng[1], Junshan Lin[2,*] and David P. Nicholls[3]

[1] *Department of Mathematics, The University of Tennessee, Knoxville, TN 37996, USA.*
[2] *Department of Mathematics and Statistics, Auburn University, Auburn, AL 36849, USA.*
[3] *Department of Mathematics, Statistics, and Computer Science, University of Illinois at Chicago, Chicago, IL 60607, USA.*

Communicated by Tao Zhou

Received 25 February 2017; Accepted (in revised version) 23 May 2017

Abstract. This paper develops an efficient and accurate numerical method for the computation of electromagnetic waves scattered by random rough surfaces. The method is based upon a combination of the Transformed Field Expansion method, which represents the solution as a provably convergent power series, and the Monte Carlo technique for sampling the probability space. The compelling aspect of the proposed method is that, at each perturbation order and every sample, the governing Transformed Field Expansion equations share the same deterministic Helmholtz operator on a deterministic domain. Thus, an LU factorization of the matrix discretization of this single operator can be employed repeatedly for all orders and every sample. Consequently, the computational complexity of the whole algorithm is significantly reduced as a result. Numerical examples are described which demonstrate the accuracy of the algorithm.

AMS subject classifications: 35J05, 35Q60, 65C05, 65C30, 78M22

Key words: Computational electromagnetic methods, random rough surface, Monte Carol method, spectral method.

1 Introduction

The scattering of electromagnetic waves from random rough surfaces has long been a subject of interest due to its significant applications in remote sensing, oceanography,

*Corresponding author. *Email addresses:* xfeng@utk.edu (X. Feng), jzl0097@auburn.edu (J. Lin), davidn@uic.edu (D. P. Nicholls)

surface plasmonics, solar cells, etc. [13, 17, 19, 23, 28, 30]. If the deviation of the surface shape from trivial (flat) is small then asymptotic techniques such as the perturbation or Kirchhoff theories can be applied to derive the analytical solutions with reasonable accuracy [5, 26, 29]. However, when the surface is a large and/or rough deviation from trivial then analytical methods are insufficient to deliver desired error tolerances and one must resort to numerical simulation of the electromagnetic wave propagation. The simplest, and most natural, numerical approach is to use the Monte Carlo (MC) method where a set of numerical solutions are obtained for independent identically distributed (*i.i.d.*) sample surface profiles which are subsequently utilized to calculate the statistics of the scattered waves [14, 18, 25]. An alternative approach is to transform the scattering problem on a random domain into a stochastic problem on a deterministic domain, which is then solved with either Monte Carlo simulations or stochastic Galerkin methods (c.f. [3, 4, 10, 34–36]). In typical simulations both of these methods become computationally intractable when a large number of degrees of freedom is required for the spatial discretization: The MC method requires solution of the full scattering problem many times with different sampling surfaces, while the stochastic Galerkin method (which is based upon the representation of the random solution by either the Karhunen-Loève or Wiener Chaos expansion) usually leads to a high-dimensional, deterministic equations that are too expensive to solve. We also refer to [7, 8] for other efficient numerical methods to solve elliptic equations with random domains.

In this paper, we propose an efficient Monte Carlo-Transformed Field Expansion (MC-TFE) method for the simulation of electromagnetic wave scattering by random rough surfaces. More precisely, a High-Order Perturbation of Surfaces (HOPS) Taylor expansion [24] is employed to represent the solution for every realization in a Monte Carlo method which is applied to sample the relevant probability space. A change of variables, which flattens the problem domain, generates a Helmholtz equation at every perturbation order with deterministic coefficients and random sources, which is posed on a deterministic domain. We apply a High Order Spectral Legendre-Galerkin method [31] to discretize the deterministic Helmholtz operator. In addition, to accelerate the algorithm, we take advantage of the fact that, at every perturbation order and every random sample, the same deterministic differential operator must be approximated. By performing an LU decomposition of the discretization matrix of the operator, all samples at every order can be obtained in an efficient way by simple forward and backward substitutions, thereby significantly reducing the computational cost. Similar expansion techniques and acceleration schemes have also been used by the authors for the modeling of waves in random media. The interested reader is referred to [11, 12] for complete details.

The rest of the paper is organized as follows. We introduce the governing equations for the scattering problem in Section 2. The computational modeling of random surfaces is briefly discussed in Section 3, and the MC-TFE method is presented and discussed in Section 4. Several numerical experiments are provided in Section 5 to demonstrate the accuracy and reliability of the method.

2 Problem formulation

We consider the scattering of electromagnetic waves by a random one-dimensional surface/curve

$$\Gamma(\omega) := \{(x,y) \mid y = g(\omega;x),\ -\infty < x < \infty\},$$

where the interface shape is a stationary Gaussian process. Here ω and (x,y) denote the random sample and the spatial variables, respectively. Fig. 1 shows one realization of a surface sample. We assume that the height of the surface is small by letting $g(\omega;x) = \varepsilon f(\omega;x)$, where $\varepsilon \in (0,1)$, and $f(\omega;x) \sim \mathcal{O}(1)$ is a stationary Gaussian process with a continuous and bounded covariance function $C(x,y) = c(x-y)$. In addition, we assume that the random surface is d-periodic so that $f(\omega;x+d) = f(\omega;x)$. We denote the domains above and below $\Gamma(\omega)$ by

$$\Omega^+(\omega) := \{y > g(\omega;x)\}, \quad \Omega^-(\omega) := \{y < g(\omega;x)\},$$

respectively. The permittivities in $\Omega^+(\omega)$ and $\Omega^-(\omega)$ are denoted by ϵ^+ and ϵ^-, respectively. It is also assumed that the permeability is μ_0 in each domain.

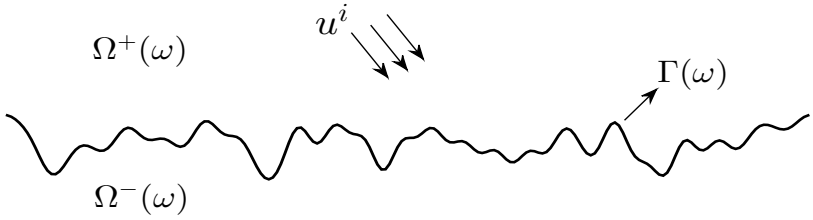

Figure 1: One realization of the random interface between the two material layers.

For concreteness we consider the case of Transverse Electric (TE) polarization (Transverse Magnetic polarization can be handled analogously) for which the electric field $E = (0,0,v)$. The random structure is illuminated by a time-harmonic plane incident wave

$$v^i = e^{i\alpha x - i\beta y},$$

where $\alpha = k^+ \sin(\theta)$, $\beta = k^+ \cos(\theta)$, θ is the angle of incidence, and k^+ is the wavenumber in the upper layer. The total field v above the surface consists of the incident wave and a scattered field $v^+(\omega;x,y)$, while below the surface the total field v is given by the transmitted field $v^-(\omega;x,y)$. In this scenario, it can be shown that the Maxwell equations reduce to the following Helmholtz equations [27]

$$\Delta v^\pm(\omega;\cdot) + (k^\pm)^2 v^\pm(\omega;\cdot) = 0, \tag{2.1}$$

where k^- is the wavenumber in the lower layer. Furthermore, the periodicity of the surface enforces the quasi-periodicity of the fields such that

$$v^\pm(\omega;x+d,y) = e^{i\alpha d} v^\pm(\omega;x,y), \tag{2.2}$$

and the scattered waves satisfy upward/downward propagating conditions. At the interface $\Gamma(\omega)$, the continuity of the electromagnetic field implies that

$$v^+(\omega;\cdot)+v^i=v^-(\omega;\cdot), \tag{2.3a}$$

$$\partial_\nu v^+(\omega;\cdot)+\partial_\nu v^i=\partial_\nu v^-(\omega;\cdot), \tag{2.3b}$$

where $\nu=(-\partial_x g(x),1)^T$ is an unnormalized normal vector.

The upward/downward propagating wave conditions can be stated with mathematical rigor by the introduction of artificial boundaries and transparent boundary conditions [1, 15]. In addition, these developments serve the useful numerical purpose of truncating the bi-infinite problem domain into one of finite extent. To summarize this procedure we consider two planes $\{y=a\}$ and $\{y=-b\}$ chosen so that $a,b>|g|_{L^\infty}$, and the resulting domain

$$\{(x,y)\,|\,-\infty<x<+\infty,\ -b<y<a\}.$$

For a fixed sample ω, the Rayleigh expansions state that the scattered field above Γ_ω can be expressed as

$$v^+=\sum_{p=-\infty}^{\infty}\hat{v}_p^+(\omega)e^{i\alpha_p x+i\beta_p^+(y-a)},$$

where

$$\alpha_p:=\alpha+(2\pi/d)p,\quad \beta_p^\pm:=\begin{cases}\sqrt{(k^\pm)^2-\alpha_p^2}, & p\in P^\pm,\\ i\sqrt{\alpha_p^2-(k^\pm)^2}, & p\notin P^\pm,\end{cases}$$

and

$$P^\pm:=\left\{p\in\mathbb{Z}\,|\,(k^\pm)^2-\alpha_p^2>0\right\},$$

which are the sets of propagating modes. The $\{\hat{v}_p^+\}$ are the Fourier coefficients of v^+ so that

$$v^+(\omega;x,a)=\sum_{p=-\infty}^{\infty}\hat{v}_p^+(\omega)e^{i\alpha_p x}.$$

It is easy to show that

$$\partial_y v^+(\omega;x,a)=\sum_{p=-\infty}^{\infty}(i\beta_p^+)\hat{v}_p^+e^{i\alpha_p x}=:T^+[v^+(\omega;x,a)],$$

which not only defines T^+ but also allows us to state the upper transparent boundary condition

$$\partial_y v^+(\omega;x,a)=T^+[v^+(\omega;x,a)]. \tag{2.4a}$$

A similar calculation at $y=-b$ yields an operator

$$T^-[v^-(\omega;x,b)]:=\sum_{p=-\infty}^{\infty}(-i\beta_p^-)\hat{v}_p^-(\omega)e^{i\alpha_p x},$$

and the lower transparent boundary condition

$$\partial_y v^-(\omega;x,b) = T^-[v^-(\omega;x,b)]. \tag{2.4b}$$

To conclude, the mathematical model in the domain $\{(x,y)\,|\,-\infty<x<\infty, -b<y<a\}$ can be described by (2.1)-(2.4b).

3 Modeling of random surfaces

To model the random surface, we adopt the well-known Karhunen-Loève expansion to represent the stationary Gaussian process $f(\omega;x)$ [20]. In more detail, since $f(\omega;x)$ is d-periodic we may expand its covariance function $c(x)$ as a Fourier series. In most applications, $c(x)$ is even and it follows that

$$c(x) = \frac{\hat{c}_0}{2} + \sum_{p=1}^{\infty} \hat{c}_p \cos\left(\frac{2p\pi x}{d}\right).$$

It can be shown explicitly that the covariance operator

$$K\varphi(x) := \int_0^d c(x-y)\varphi(y)dy,$$

possesses the eigenvalues $\lambda_j = d\hat{c}_j/2$, $j=0,1,2,\cdots$. The corresponding eigenfunctions are

$$\varphi_j(x) = \begin{cases} \sqrt{\dfrac{1}{d}}, & j=0, \\ \sqrt{\dfrac{2}{d}}\cos\left(\dfrac{2j\pi x}{d}\right), & j>1, \text{ even}, \\ \sqrt{\dfrac{2}{d}}\sin\left(\dfrac{2j\pi x}{d}\right), & j>1, \text{ odd}. \end{cases}$$

The Karhunen-Loève representation of the random process $f(\omega;x)$ is given by

$$\begin{aligned} f(\omega;x) = &\overline{f}(x) + \sqrt{\lambda_0}\xi_0(\omega)\sqrt{\frac{1}{d}} \\ &+ \sum_{j=1}^{\infty}\sqrt{\lambda_j}\left[\xi_{j,s}(\omega)\sqrt{\frac{2}{d}}\sin\left(\frac{2j\pi x}{d}\right) + \xi_{j,c}(\omega)\sqrt{\frac{2}{d}}\cos\left(\frac{2j\pi x}{d}\right)\right], \end{aligned}$$

where $\overline{f}(x)$ is some deterministic function, $\{\lambda_j\}_{j=0}^{\infty}$ are the eigenvalues of the covariance operator K, and ξ_0, $\xi_{j,c}$ and $\xi_{j,s}$ are *i.i.d.* Gaussian random variables with zero mean and unit covariance.

Two widely used covariance functions for the modeling of rough surfaces are $c(x-y) = \sigma_0^2\exp(-|x-y|^q/\ell^q)$ for $q=1,2$, where σ_0 is the standard deviation (or root mean

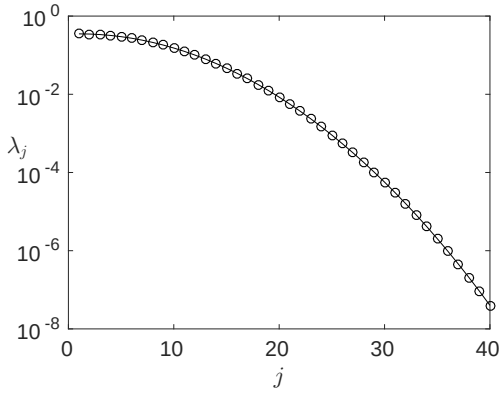

Figure 2: Eigenvalues for the Gaussian covariance operator when $d=10\pi$ and $\ell=1$.

square of the surface) and ℓ is the correlation length [26]. Here we consider a Gaussian random surface by letting $c(x-y)=\sigma_0^2\exp(|x-y|^2/\ell^2)$ and $0<\ell\ll d$. In practical computations, a finite-term Karhunen-Loève expansion is adopted, and the contribution from the truncated terms is negligibly small. Fig. 2 shows the decay of the eigenvalues λ_j when the period is $d=10\pi$, the root mean square $\sigma_0=1$, and the correlation length is $\ell=1$. We see that only the first 30 terms are needed to represent the random surface with an accuracy of 10^{-2}.

4 The Monte Carlo-Transformed Field Expansion method

The Monte Carlo-Transformed Field Expansion (MC-TFE) method is based upon the following ingredients: (i) a simple domain-flattening change of variables; (ii) a High-Order Perturbation of Surfaces (HOPS) expansion of the solution; (iii) Monte Carlo sampling of the probability space and an acceleration strategy for solving the discretized problems for all samples. For each sample ω, (i) and (ii) have the same spirit as the deterministic TFE method, which has been studied extensively in [15, 23, 24]. Recently, the TFE approach has also been applied to solve the inverse surface scattering problem [2]. We describe the process briefly below for the purpose of completeness. The interested reader is referred to [15,23,24] for full details.

4.1 Change of variables

To flatten the interface $\Gamma(\omega)$, for each sample ω, the TFE change of variables is specified by $x'=x$ and

$$y'=\begin{cases} a\left(\dfrac{y-g}{a-g}\right), & g<y<a, \\ b\left(\dfrac{y-g}{b+g}\right), & -b<y<g, \end{cases}$$

which implies that $x=x'$ and

$$y=\begin{cases}\left(\dfrac{a-g}{a}\right)y'+g, & 0<y'<a,\\ \left(\dfrac{b+g}{b}\right)y'+g, & -b<y'<0.\end{cases}$$

These allow us to define the transformed fields

$$u^+(\omega;x',y'):=v^+\left(\omega;x',\left(\frac{a-g}{a}\right)y'+g\right),$$

and

$$u^-(\omega;x',y'):=v^-\left(\omega;x',\left(\frac{b+g}{b}\right)y'+g\right).$$

If we denote $\Delta':=\partial^2_{x'}+\partial^2_{y'}$, then (2.1)-(2.4b) become

$$\Delta' u^+(\omega;\cdot)+(k^+)^2u^+(\omega;\cdot)=F^+(\omega;\cdot), \qquad 0<y'<a, \tag{4.1a}$$
$$\Delta' u^-(\omega;\cdot)+(k^-)^2u^-(\omega;\cdot)=F^-(\omega;\cdot), \quad -b<y'<0, \tag{4.1b}$$
$$\partial_{y'}u^+(\omega;x',a)-T^+[u^+(\omega;x',a)]=J^+(\omega;x'), \tag{4.1c}$$
$$\partial_{y'}u^-(\omega;x',-b)-T^-[u^-(\omega;x',-b)]=J^-(\omega;x'), \tag{4.1d}$$
$$u^+(\omega;x',0)-u^-(\omega;x',0)=-\phi(\omega;x'), \tag{4.1e}$$
$$\partial_{y'}u^+(\omega;x',0)-\partial_{y'}u^-(\omega;x',0)=Q(\omega;x'), \tag{4.1f}$$
$$u^\pm(\omega;x'+d,y')=e^{i\alpha d}u^\pm(\omega;x',y'). \tag{4.1g}$$

In the above equations,

$$F^\pm(\omega;\cdot)=\partial_{x'}F^\pm_x(\omega;\cdot)+\partial_{y'}F^\pm_y(\omega;\cdot)+F^\pm_h(\omega;\cdot),$$

where

$$\begin{aligned}F^+_x=&\frac{2}{a}g\partial_{x'}u^+-\frac{1}{a^2}g^2\partial_{x'}u^++\frac{a-y'}{a}(\partial_{x'}g)\partial_{y'}u^+\\&-\frac{a-y'}{a^2}g(\partial_{x'}g)\partial_{y'}u^+,\\F^+_y=&\frac{a-y'}{a}(\partial_{x'}g)\partial_{x'}u^+-\frac{a-y'}{a^2}g(\partial_{x'}g)\partial_{x'}u^+\\&-\frac{(a-y')^2}{a^2}(\partial_{x'}g)^2\partial_{y'}u^+,\\F^+_h=&(k^+)^2\frac{2}{a}gu^+-(k^+)^2\frac{1}{a^2}g^2u^+-\frac{1}{a}(\partial_{x'}g)\partial_{x'}u^+\\&+\frac{1}{a^2}g(\partial_{x'}g)\partial_{x'}u^++\frac{a-y'}{a^2}(\partial_{x'}g)^2\partial_{y'}u^+,\end{aligned}$$

and

$$\begin{aligned}
F_x^- =& -\frac{2}{b}g\partial_{x'}u^- - \frac{1}{b^2}g^2\partial_{x'}u^- + \frac{b+y'}{b}(\partial_{x'}g)\partial_{y'}u^- \\
&+ \frac{b+y'}{b^2}g(\partial_{x'}g)\partial_{y'}u^-, \\
F_y^- =& \frac{b+y'}{b}(\partial_{x'}g)\partial_{x'}u^- + \frac{b+y'}{b^2}g(\partial_{x'}g)\partial_{x'}u^- \\
&- \frac{(b+y')^2}{b^2}(\partial_{x'}g)^2\partial_{y'}u^-, \\
F_h^- =& -(k^-)^2\frac{2}{b}gu^- - (k^-)^2\frac{1}{b^2}g^2u^- + \frac{1}{b}(\partial_{x'}g)\partial_{x'}u^- \\
&+ \frac{1}{b^2}g(\partial_{x'}g)\partial_{x'}u^- - \frac{b+y'}{b^2}(\partial_{x'}g)^2\partial_{y'}u^-.
\end{aligned}$$

Furthermore,

$$\begin{aligned}
J^+ &= -\frac{1}{a}gT^+[u^+], \\
J^- &= \frac{1}{b}gT^-[u^-], \\
\phi &= -e^{i\alpha x - i\beta g},
\end{aligned}$$

and

$$\begin{aligned}
Q = \frac{1}{ab}\Big\{ & (ab+ag-bg-g^2)(i\alpha\partial_{x'}g+i\beta)\phi - ag\partial_{y'}u^+ \\
& + (\partial_{x'}g)(b+g)(a-g)\partial_{x'}u^+ - (\partial_{x'}g)^2a(b+g)\partial_{y'}u^+ \\
& - bg\partial_{y'}u^- - (\partial_{x'}g)(b+g)(a-g)\partial_{x'}u^- \\
& + (\partial_{x'}g)^2b(a-g)\partial_{y'}u^- \Big\}.
\end{aligned}$$

Remark 4.1. Since $F^\pm$ and $J^\pm$ depend on $v^\pm$ and g, then the PDEs in (4.1) are genuine random PDEs.

4.2 HOPS expansion of the solution

To pursue the High-Order Perturbation of Surfaces (HOPS) method, recall that $g=\varepsilon f$, where f is sufficiently smooth (C^2 continuity suffices, though Lipschitz profiles can also be accommodated [16,22]). For each fixed sample ω, we expand the solution as

$$u^\pm(\omega;\cdot) = \sum_{n=0}^{\infty}\varepsilon^n u_n^\pm(\omega;\cdot). \tag{4.2}$$

By substituting this form into (4.1) and collecting the terms at each order in ε^n, it can be shown that for $n \geq 0$

$$\Delta' u_n^+(\omega;\cdot) + (k^+)^2 u_n^+(\omega;\cdot) = F_n^+(\omega;\cdot), \qquad 0 < y' < a, \tag{4.3a}$$
$$\Delta' u_n^-(\omega;\cdot) + (k^-)^2 u_n^-(\omega;\cdot) = F_n^-(\omega;\cdot), \quad -b < y' < 0, \tag{4.3b}$$
$$\partial_{y'} u_n^+(\omega;x',a) - T^+[u_n^+(\omega;x',a)] = J_n^+(\omega;x'), \tag{4.3c}$$
$$\partial_{y'} u_n^-(\omega;x',-b) - T^-[u_n^-(\omega;x',-b)] = J_n^-(\omega;x'), \tag{4.3d}$$
$$u_n^+(\omega;x',0) - u_n^-(\omega;x',0) = \phi_n(\omega;x'), \tag{4.3e}$$
$$\partial_{y'} u_n^+(\omega;x',0) - \partial_{y''} u_n^-(\omega;x',0) = Q_n(\omega;x'). \tag{4.3f}$$
$$u_n^\pm(\omega;x'+d,y') = e^{i\alpha d} u_n^\pm(\omega;x',y'). \tag{4.3g}$$

The source terms are given by

$$F_n^\pm(\omega;\cdot) = \partial_{x'} F_{n,x}^\pm(\omega;\cdot) + \partial_{y'} F_{n,y}^\pm(\omega;\cdot) + F_{n,h}^\pm(\omega;\cdot),$$

where

$$\begin{aligned}
F_{n,x}^+ &= \frac{2}{a} f \partial_{x'} u_{n-1}^+ - \frac{1}{a^2} f^2 \partial_{x'} u_{n-2}^+ + \frac{a-y'}{a} (\partial_{x'} f) \partial_{y'} u_{n-1}^+ \\
&\quad - \frac{a-y'}{a^2} f (\partial_{x'} f) \partial_{y'} u_{n-2}^+, \\
F_{n,y}^+ &= \frac{a-y'}{a} (\partial_{x'} f) \partial_{x'} u_{n-1}^+ - \frac{a-y'}{a^2} f (\partial_{x'} f) \partial_{x'} u_{n-2}^+ \\
&\quad - \frac{(a-y')^2}{a^2} (\partial_{x'} f)^2 \partial_{y'} u_{n-2}^+, \\
F_{n,h}^+ &= (k^+)^2 \frac{2}{a} f u_{n-1}^+ - \frac{1}{a} (\partial_{x'} f) \partial_{x'} u_{n-1}^+ - (k^+)^2 \frac{1}{a^2} f^2 u_{n-2}^+ \\
&\quad + \frac{1}{a^2} f (\partial_{x'} f) \partial_{x'} u_{n-2}^+ + \frac{a-y'}{a^2} (\partial_{x'} f)^2 \partial_{y'} u_{n-2}^+,
\end{aligned}$$

and similar expressions for $F_{n,x}^-$, $F_{n,y}^-$, and $F_{n,h}^-$ can be derived. Furthermore,

$$\begin{aligned}
J_n^+ &= -\frac{1}{a} f T^+[u_{n-1}^+], \\
J_n^- &= \frac{1}{b} f T^-[u_{n-1}^-], \\
\phi_n &= (-1)^{n+1} \frac{(i\beta f)^n}{n!} e^{i\alpha x},
\end{aligned}$$

and

$$\begin{aligned}Q_n=\frac{1}{ab}\{&-iab\beta\phi_n-iab\alpha\partial_{x'}f\phi_{n-1}-i\beta(a-b)f\phi_{n-1}\\&-i\alpha(a-b)f\partial_{x'}f\phi_{n-2}+i\beta f^2\phi_{n-2}+i\alpha\partial_{x'}ff^2\phi_{n-3}\\&-af\partial_{y'}u^+_{n-1}+ab\partial_{x'}f\partial_{x'}u^+_{n-1}+(a-b)f\partial_{x'}f\partial_{x'}u^+_{n-2}\\&-\partial_{x'}ff^2\partial_{x'}u^+_{n-3}-ab(\partial_{x'}f)^2\partial_{y'}u^+_{n-2}-a(\partial_{x'}f)^2f\partial_{y'}u^+_{n-3}\\&-bf\partial_{y'}u^-_{n-1}-ab\partial_{x'}f\partial_{x'}u^-_{n-1}-(a-b)f\partial_{x'}f\partial_{x'}u^-_{n-2}\\&+\partial_{x'}ff^2\partial_{x'}u^-_{n-3}+ab(\partial_{x'}f)^2\partial_{y'}u^-_{n-2}-bf(\partial_{x'}f)^2\partial_{y'}u^-_{n-3}\}.\end{aligned}$$

Remark 4.2. In the above formulas, we set $u^\pm_{-1}=u^\pm_{-2}=u^\pm_{-3}=0$. The source term $F^\pm_n$ in (4.3) depends only on the two previous solution orders $u^\pm_{n-1}$ and $u^\pm_{n-2}$, and Q_n depends only on the previous three orders $u^\pm_{n-1}$, $u^\pm_{n-2}$, and $u^\pm_{n-3}$.

4.3 The Monte Carlo-Transformed Field Expansion method

We are now in a position to introduce the Monte Carlo-Transformed Field Expansion (MC-TFE) method for approximating the solution of the problem (2.1)-(2.4b). The method is based upon the HOPS expansion (4.2), and for each Taylor order, u_n, the Legendre-Galerkin method [31] is applied to discretize (4.3a)-(4.3f). Following this, the classical Monte Carlo method is employed to sample the probability space and to compute the statistics of the numerical solution. It should be pointed out that more efficient sampling techniques such as quasi-Monte Carlo methods or stochastic collocation methods (cf. [6, 21]) can also be applied, but we omit the discussion here for conciseness. Very importantly, our scheme can be significantly accelerated by noting that the *same* deterministic differential operator is inverted on the *same* deterministic domain for all Taylor orders and all samples. This is discussed in detail below.

Let M be a (large) positive integer which denotes the number of realizations for the Monte Carlo method. For each $m=1,2,\cdots,M$, we sample *i.i.d.* realizations of the source function $F^\pm_n(\omega_m;\cdot)$ and the boundary terms $J^\pm_n(\omega_m;\cdot)$, $\phi_n(\omega_m;\cdot)$, and $Q_n(\omega_m;\cdot)$. Due to quasi-periodicity of $u^\pm_n$, we may expand

$$u^\pm_n(\omega_m;x',y')=\sum_{p=-\infty}^{\infty}u^\pm_{n,p}(\omega_m;y')e^{i\alpha_p x'}.$$

Correspondingly,

$$\begin{aligned}F^\pm_n(\omega_m;x',y')&=\sum_{p=-\infty}^{\infty}F^\pm_{n,p}(\omega_m;y')e^{i\alpha_p x'},\\J^\pm_n(\omega_m;x')&=\sum_{p=-\infty}^{\infty}J^\pm_{n,p}(\omega_m)e^{i\alpha_p x'},\end{aligned}$$

$$\phi_n(\omega_m;x') = \sum_{p=-\infty}^{\infty} \phi_{n,p}(\omega_m) e^{i\alpha_p x'},$$

$$Q_n(\omega_m;x') = \sum_{p=-\infty}^{\infty} Q_{n,p}(\omega_m;y') e^{i\alpha_p x'}.$$

By substituting these into (4.3), we obtain the following set of two-point boundary value problems for the functions $u^{\pm}_{n,p}(\omega;y')$,

$$\frac{d^2u^+_{n,p}}{dy'^2} + (\beta^+_p)^2 u^+_{n,p} = F^+_{n,p}(\omega_m;y'), \qquad 0<y'<a, \tag{4.4a}$$

$$\frac{d^2u^+_{n,p}}{dy'^2} + (\beta^-_p)^2 u^-_{n,p} = F^-_{n,p}(\omega_m;y'), \quad -b<y'<0, \tag{4.4b}$$

$$\frac{du^+_{n,p}}{dy'}(\omega_m;a) - i\beta^+_p u^+_{n,p}(\omega_m;a) = J^+_{n,p}(\omega_m), \tag{4.4c}$$

$$\frac{du^+_{n,p}}{dy'}(\omega_m;-b) + i\beta^-_p u^-_{n,p}(\omega_m;-b) = J^-_{n,p}(\omega_m), \tag{4.4d}$$

$$u^+_{n,p}(\omega_m;0) - u^-_{n,p}(\omega_m;0) = \phi_{n,p}(\omega_m), \tag{4.4e}$$

$$\frac{du^+_{n,p}}{dy'}(\omega_m;0) - \frac{du^-_{n,p}}{dy'}(\omega_m;0) = Q_{n,p}(\omega_m). \tag{4.4f}$$

To solve for $u^{\pm}_{n,p}$ we write

$$u^{\pm}_{n,p} = u^{\pm,1}_{n,p} + u^{\pm,2}_{n,p},$$

where $u^{\pm,1}_{n,p}$ is the solution of (4.4) with homogeneous boundary conditions (i.e., $J^{\pm}_{n,p} \equiv \phi_{n,p} \equiv Q_{n,p} \equiv 0$) and $u^{\pm,2}_{n,p}$ is the solution of (4.4) with $F^{\pm}_{n,p} \equiv 0$. Note that $u^{\pm,2}_{n,p}$ can be calculated explicitly [15]. To obtain $u^{\pm,1}_{n,p}$ various numerical methods can be applied to solve the above two-point boundary problem, and here we use the Legendre-Galerkin method. For this, let P_r be the space of polynomials of degree at most r in the regions $(-b,0)$ and $(0,a)$ respectively, and

$$Y_r = \{u |\ u \in P_r, (u' - i\beta^+_p u)(a) = (u' + i\beta^-_p u)(-b) = 0\}.$$

It can be shown that [15]

$$Y_r = \text{span}\{\phi_0, \phi_1, \ldots, \phi_{2r-2}\},$$

where ϕ_j are Legendre polynomials. Then the Legendre-Galerkin method is to find $\widetilde{u}^{\pm,1}_{n,p} \in Y_r$ such that

$$-\left((\widetilde{u}^{\pm,1}_{n,p})', v_r'\right) + \beta_p^2 (\widetilde{u}^{\pm,1}_{n,p}, v_r) = (F^{\pm}_{n,p}, v_r), \qquad \forall v_r \in Y_r, \tag{4.5}$$

where $(\cdot,\cdot)$ denotes the L^2-inner product. For each p this leads to $(2r-1)$ linear equations to solve

$$A_p \widetilde{u}^1_{n,p} = f_{n,p}.$$

We refer the interested reader to [15] for the detailed specification of the matrix A_p.

We denote the numerical solution of (4.4) by $\widetilde{u}^{\pm}_{n,p}$, which is the sum of $\widetilde{u}^{\pm,1}_{n,p}$ and $u^{\pm,2}_{n,p}$, and approximate the expectation $\mathbb{E}(u^{\pm}_n)$ of each Taylor order $u^{\pm}_n$ by the sampling average

$$\overline{u}^{\pm}_n = \frac{1}{M}\sum_{m=1}^{M}\sum_{p=-N_x}^{N_x}\widetilde{u}^{\pm}_{n,p}(\omega_m;y')e^{i\alpha_p x}.$$

Consequently, by virtue of (4.2), the algorithm yields an approximation of $\mathbb{E}(u^{\pm})$ given by

$$\overline{U}^{\pm} = \frac{1}{M}\sum_{m=1}^{M}\sum_{n=0}^{N}\varepsilon^n\left(\sum_{p=-N_x}^{N_x}\widetilde{u}^{\pm}_{n,p}(\omega_m;y')e^{i\alpha_p x}\right). \tag{4.6}$$

Similarly, the standard deviation of the sampled solution, which is denoted by $\sigma^{\pm}_U$, can be computed by using the formula

$$(\sigma^{\pm}_U)^2 = \frac{1}{M}\sum_{j=1}^{M}\left(\sum_{n=0}^{N}\varepsilon^n\sum_{p=-N_x}^{N_x}\widetilde{u}^{\pm}_{n,p}(\omega_m;y')e^{i\alpha_p x} - U^{\pm}\right)^2,$$

and no further computational cost is required.

Importantly, we observe that from (4.4a) and (4.4b), for each fixed p, all Taylor orders for all samples share the same deterministic elliptic operator $\partial^2_{y'}+(\beta^{\pm}_p)^2$ (generating the same discretized matrix A_p). Using this crucial fact, a LU decomposition of A_p leads to a tremendous savings in the computational cost. In more detail, for each p we factor A_p into lower and upper triangular matrices, L_p and U_p, which are stored and used repeatedly to obtain the solution at each Taylor order and every sample. In contrast to a full direct linear solver with $\mathcal{O}(r^3)$ computational complexity, our MC-TFE algorithm requires only $\mathcal{O}(r^2)$ computational cost to calculate $\widetilde{u}^{\pm}_{n,p}(\omega,\cdot)$ for each n, p and ω_m by simple forward and backward substitutions. The precise description of this procedure is given in the following Main Algorithm.

Set $\overline{U}^{\pm}(\cdot)=0$ (initializing)

For $m=1,2,\cdots,M$ (sampling)

Generate ω_m

Set $U^{\pm}_N(\omega_m,\cdot)=\tilde{u}^{\pm}_0(\omega_m,\cdot)$ (initializing)

For $n=1,2,\cdots,N$ (for each mode)

Evaluate $F^{\pm}_{n,p}(\omega_m;\cdot)$, $J^{\pm}_{n,p}(\omega_m;\cdot)$, $\phi^{\pm}_{n,p}(\omega_m;\cdot)$, and $Q^{\pm}_{n,p}(\omega_m;\cdot)$ by the DFT.

For $p=-N_x,\cdots,0,1,\cdots,N_x$

Solve $L_p v_{n,p}=f_{n,p}$ and $U_p\widetilde{u}^{\pm,1}_{n,p}=v_{n,p}$.

$\widetilde{u}^{\pm}_{n,p}\leftarrow\widetilde{u}^{\pm,1}_{n,p}+\widetilde{u}^{\pm,2}_{n,p}$.

End For

$\widetilde{u}_n^{\pm} \leftarrow \sum_{p=-N_x}^{N_x} \widetilde{u}_{n,p}^{\pm}(\omega_m;y')e^{i\alpha_p x}$.

Set $U_N^{\pm}(\omega_m,\cdot) \leftarrow U_N^{\pm}(\omega_m,\cdot)+\varepsilon^n \widetilde{u}_n^{\pm}$.

End For

$\overline{U}^{\pm}(\cdot) \leftarrow \overline{U}^{\pm}(\cdot)+\frac{1}{M}U_N^{\pm}(\omega_m,\cdot)$.

End For

Return $\overline{U}^{\pm}$.

Since the implementation of forward and backward substitutions for solving $L_p v_{n,p}=f_{n,p}$ and $U_p \widetilde{u}_{n,p}^{\pm,1}=v_{n,p}$ respectively only requires $\mathcal{O}(r^2)$ multiplications, the cost for obtaining coefficients $\widetilde{u}_{n,p}^{\pm}$ for all p, n and ω_m is $\mathcal{O}(MNN_x r^2)+\mathcal{O}(r^3)$. On the other hand, the evaluation of coefficients $F_{n,p}^{\pm}(\omega_m;\cdot)$, $J_{n,p}^{\pm}(\omega_m;\cdot)$, $\phi_{n,p}^{\pm}(\omega_m;\cdot)$, $Q_{n,p}^{\pm}(\omega_m;\cdot)$ and the solution $\widetilde{u}^{\pm}$ by FFT require $\mathcal{O}(MN\cdot rN_x \ln N_x)$ multiplications for all samples and perturbation orders. Consequently, the overall computational cost for the Main Algorithm is $\mathcal{O}(MNN_x\cdot(r^2+r\ln N_x))+\mathcal{O}(r^3)$. As a comparison, we note that if a brute-force Monte Carlo method and standard discretization schemes such as finite element method is applied for solving the scattering problem over the domain at each sample, the total computational cost would be $\mathcal{O}(M\cdot(\tilde{N}_x\tilde{N}_y)^3)$, where $\tilde{N}_x$ and $\tilde{N}_y$ are the number of discretization points along the x and y directions respectively. Typically, $\tilde{N}_x \geq N_x$ and $\tilde{N}_y \geq r$ is required for the finite element discretization in order to obtain the same order of accuracy as that of the spectral method. Therefore, we see that the cost is significantly reduced by the MC-TFE method. Finally, we remark that the Monte Carlo sampling process can be performed in parallel.

5 Numerical results

We now present a series of numerical examples to illustrate the accuracy and efficiency of the proposed method. In order to establish the reliability of our method we recall a common diagnostic of convergence, the energy defect [27]. For this we recall the Rayleigh expansions for the scattered wave:

$$v^+(\omega;x,y)=\sum_{p=-\infty}^{\infty}\hat{v}_p^+(\omega)e^{i\alpha_p x+i\beta_p^+ y}, \qquad y>a,$$

$$v^-(\omega;x,y)=\sum_{p=-\infty}^{\infty}\hat{v}_p^-(\omega)e^{i\alpha_p x-i\beta_p^- y}, \qquad y<-b.$$

From these we define the mean reflectivity and transmittance by

$$\overline{R}=\frac{1}{M}\sum_{m=1}^{M}\sum_{p\in P^+}\frac{\beta_p^+}{\beta_0^+}\left|\hat{v}_p^+(\omega_m)\right|^2,$$

and

$$\overline{T}=\frac{1}{M}\sum_{m=1}^{M}\sum_{p\in P^-}\frac{\beta_p^-}{\beta_0^+}\left|\hat{v}_p^-(\omega_m)\right|^2,$$

respectively. The standard deviation of the reflectivity and the transmittance, σ_R and σ_T, are given by

$$\sigma_R^2=\frac{1}{M}\sum_{m=1}^{M}\left(\frac{\beta_p^+}{\beta_0^+}\left|\hat{v}_p^+(\omega_m)\right|^2-\overline{R}\right)^2,$$

and

$$\sigma_T^2=\frac{1}{M}\sum_{m=1}^{M}\left(\frac{\beta_p^-}{\beta_0^+}\left|\hat{v}_p^-(\omega_m)\right|^2-\overline{T}\right)^2,$$

respectively.

The principle of conservation of energy for each sample ω [27] states

$$\sum_{p\in P^+}\frac{\beta_p^+}{\beta_0^+}\left|\hat{v}_p^+(\omega)\right|^2+\sum_{p\in P^-}\frac{\beta_p^-}{\beta_0^+}\left|\hat{v}_p^-(\omega)\right|^2=1,$$

and we define the energy defect for each sample by

$$e(\omega):=\sum_{p\in P^+}\frac{\beta_p^+}{\beta_0^+}\left|\hat{v}_p^+(\omega)\right|^2+\sum_{p\in P^-}\frac{\beta_p^-}{\beta_0^+}\left|\hat{v}_p^-(\omega)\right|^2-1.$$

The mean energy defect and the standard deviation are denoted by $\overline{e}$ and σ_e respectively. It is clear that $\overline{e}=\overline{R}+\overline{T}-1$.

For all of the numerical examples presented below, we have set $k^+=1$ and $k^-=2$, period $d=10\pi$, and $a=b=2$. So, the problem (2.1)-(2.4b) is solved over the bounded domain $\{(x,y)|0<x<10\pi,-2<y<2\}$. In the Karhunen-Loève representation, P is chosen such that $|\lambda_j^{P+1}|<10^{-4}$ and the representation has two digits of accuracy, where λ_j is the eigenvalue of the covariance operator K. Finally, we also set the number of realizations $M=10^4$ which yields two digits of accuracy in sampling the probability space.

5.1 Accuracy of the numerical algorithm

The random surfaces are modeled by the Karhunen-Loève expansion described in Section 3, with the covariance function $c(x-y)=(1/3)^2\cdot\exp(-|x-y|^2/\ell^2)$. Here we choose

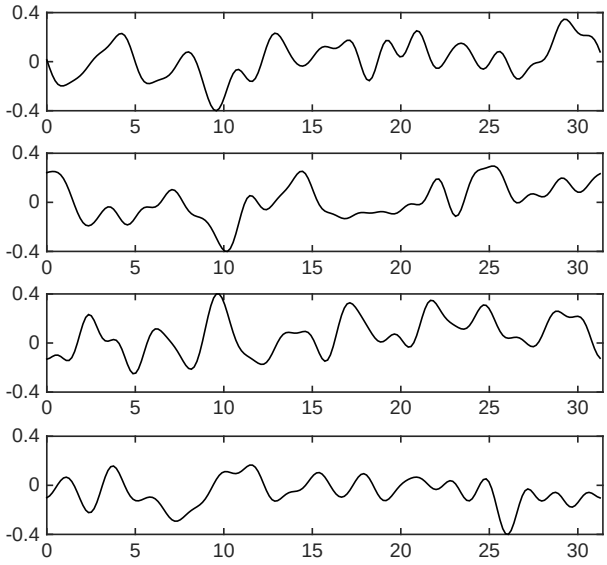

Figure 3: Four realizations of random surfaces when $\varepsilon=0.4$.

the correlation length $\ell=1$, and Fig. 3 shows four realizations of random surfaces when $\varepsilon=0.4$.

In the following numerical simulations, the number of Taylor orders is set to $N=10$. In addition, in order to resolve the oscillations of the waves with sufficient accuracy, we set the lateral and vertical discretizations at $N_x=400$ and $r=40$, respectively. Fig. 4 demonstrates the computed mean and the standard deviation of the reflectivity for different incident angles when the magnitudes of the surface perturbations are $\varepsilon=0.2$, 0.4, 0.6 and 0.8, respectively. Fig. 5 demonstrates the computed mean and the standard deviation of the transmittance for different incident angles and for different magnitudes of surface perturbation. We observe that, for a fixed incident angle, the standard deviation of both the reflectivity and transmittance increases as ε increases. To test the accuracy of the algorithm, the mean $\overline{e}$ and the standard deviation σ_e of the energy defect are calculated, and are shown in Fig. 6. We note that as ε increases, the accuracy of the algorithm deteriorates which is to be expected as we are moving away from the center of the disk of convergence of the HOPS expansion at $\varepsilon=0$. In addition, $\overline{e}$ and σ_e become larger as the incident angle increases to the very challenging regime of grazing incidence. For instance, when $\varepsilon=0.8$ we find $\overline{e}>0.05$ if the incident angle $\theta>50^o$.

5.2 Performance of the algorithm: Numerical parameters

To test the accuracy of the algorithm as the number of Taylor orders N is increased, we consider normally incident waves, and fix $N_x=400$ and $r=40$ in the numerical calcu-

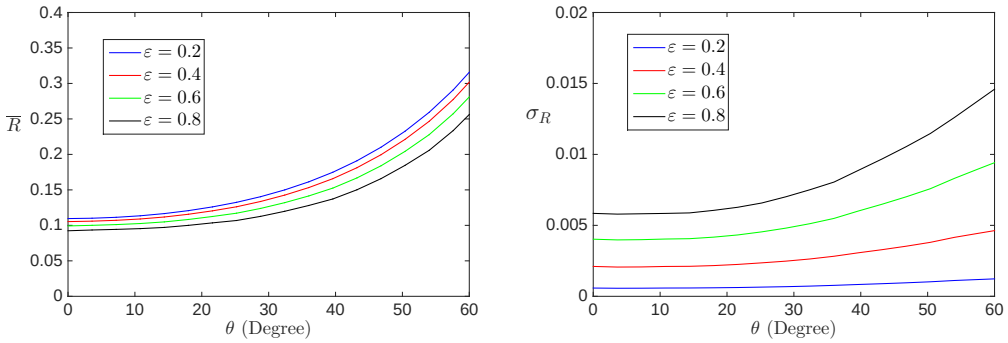

Figure 4: Mean and standard deviation of the reflectivity for $\theta \in [0,60^o]$ and $\varepsilon = 0.2,\ 0.4,\ 0.6,\ 0.8$.

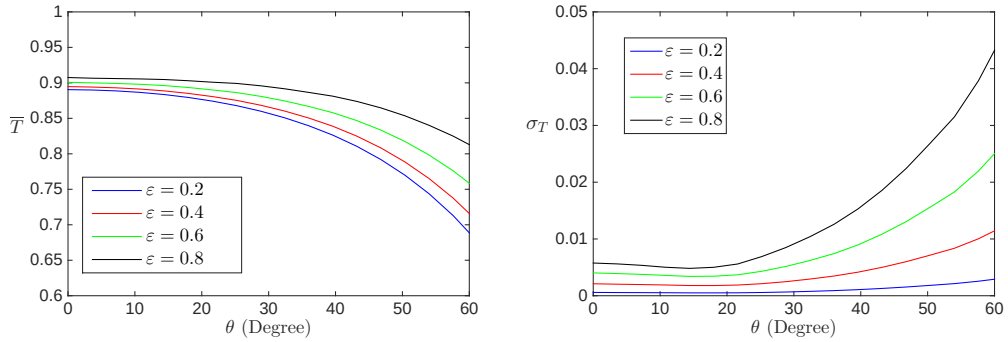

Figure 5: Mean and standard deviation of the transmittance for $\theta \in [0,60^o]$ and $\varepsilon = 0.2,\ 0.4,\ 0.6,\ 0.8$.

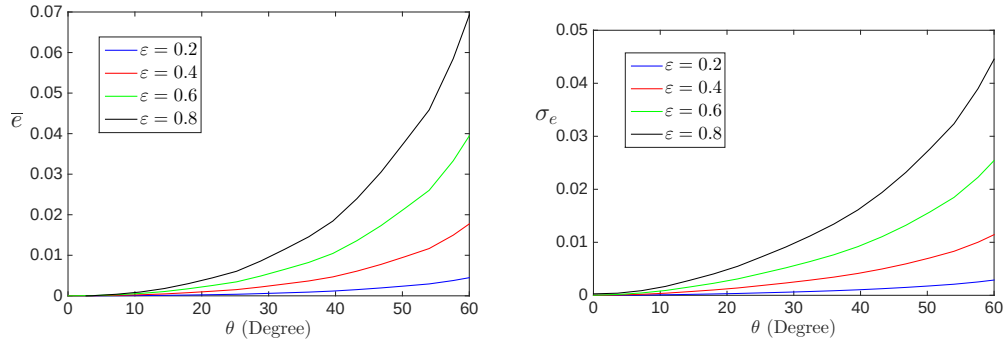

Figure 6: Mean and standard deviation of the energy defect for $\theta \in [0,60^o]$ $\varepsilon = 0.2,\ 0.4,\ 0.6,\ 0.8$.

lations. The magnitude of the mean energy defect $|\overline{e}|$ and the standard deviation σ_e for various ε and different values of N are displayed in Tables 1 and 2. For a fixed ε, as expected, we observe that higher accuracy is achieved if more Taylor orders in (4.2) are retained. On the other hand, for fixed N, a smaller perturbation of the random rough surface yields a more accurate numerical solution.

Table 1: $|\overline{e}|$ for $\varepsilon=0.2,0.4,0.6,0.8$ and $N=2,4,6$.

ε	$N=2$	$N=4$	$N=6$
0.2	8.53×10^{-5}	7.42×10^{-7}	5.00×10^{-9}
0.4	1.33×10^{-3}	4.50×10^{-5}	1.81×10^{-8}
0.6	6.74×10^{-3}	4.68×10^{-4}	1.89×10^{-7}
0.8	2.13×10^{-2}	2.28×10^{-3}	5.08×10^{-5}

Table 2: σ_e for $\varepsilon=0.2,0.4,0.6,0.8$ and $N=2,4,6$.

ε	$N=2$	$N=4$	$N=6$
0.2	2.06×10^{-4}	4.64×10^{-6}	5.38×10^{-7}
0.4	1.73×10^{-3}	9.36×10^{-5}	7.54×10^{-6}
0.6	6.30×10^{-3}	7.42×10^{-4}	1.12×10^{-4}
0.8	1.63×10^{-2}	3.15×10^{-3}	8.51×10^{-4}

5.3 Performance of the algorithm: Correlation length

We now discuss the performance of our algorithm as the correlation length is varied. For this we consider random surfaces with correlation lengths $\ell=0.5$, 1.0 and 2.0; Fig. 7 shows one realization of each with $\varepsilon=0.8$. We observe that the surface becomes "rougher" as the correlation length decreases.

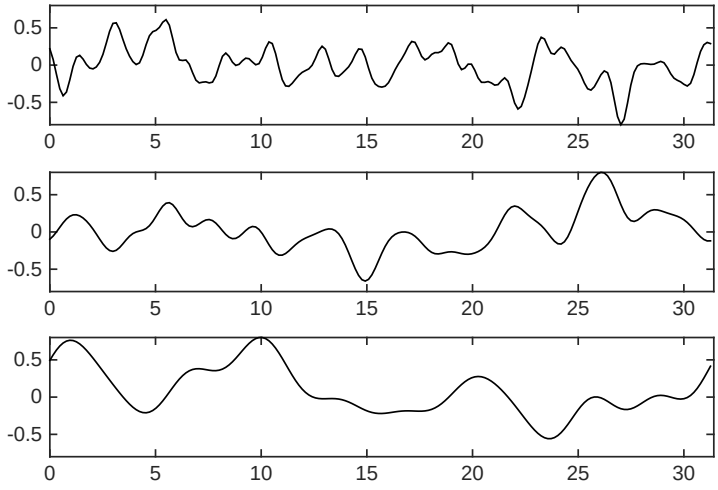

Figure 7: Three realizations of random surfaces with correlation lengths $\ell=0.5$ (top), $\ell=1.0$ (middle) and $\ell=2.0$ (bottom), respectively, for $\varepsilon=0.8$.

Table 3: $|\overline{e}|$ for $\varepsilon=0.2,0.4,0.6,0.8$ and $\ell=0.5,1.0,2.0$. The incident angle was $\theta=0$.

ε	$\ell=0.5$	$\ell=1.0$	$\ell=2.0$
0.2	1.00×10^{-9}	7.82×10^{-12}	3.37×10^{-13}
0.4	2.60×10^{-7}	2.59×10^{-8}	1.78×10^{-9}
0.6	3.24×10^{-5}	3.53×10^{-6}	1.72×10^{-7}
0.8	4.77×10^{-4}	1.02×10^{-4}	1.71×10^{-6}

Table 4: σ_e for $\varepsilon=0.2,0.4,0.6,0.8$ and $\ell=0.5,1.0,2.0$. The incident angle was $\theta=0$.

ε	$\ell=0.5$	$\ell=1.0$	$\ell=2.0$
0.2	1.00×10^{-7}	4.61×10^{-11}	3.79×10^{-12}
0.4	2.54×10^{-6}	7.50×10^{-7}	1.10×10^{-7}
0.6	1.25×10^{-4}	1.13×10^{-5}	1.71×10^{-6}
0.8	4.08×10^{-3}	2.75×10^{-4}	1.90×10^{-5}

Table 5: $|\overline{e}|$ for $\varepsilon=0.2,0.4,0.6,0.8$ and $\ell=0.5,1.0,2.0$. The incident angle was $\theta=30^o$.

ε	$\ell=0.5$	$\ell=1.0$	$\ell=2.0$
0.2	4.45×10^{-4}	6.06×10^{-4}	7.01×10^{-4}
0.4	1.75×10^{-3}	2.41×10^{-3}	2.84×10^{-3}
0.6	3.79×10^{-3}	5.40×10^{-3}	6.35×10^{-3}
0.8	8.91×10^{-3}	9.50×10^{-3}	1.12×10^{-2}

Table 6: σ_e for $\varepsilon=0.2,0.4,0.6,0.8$ and $\ell=0.5,1.0,2.0$. The incident angle was $\theta=30^o$.

ε	$\ell=0.5$	$\ell=1.0$	$\ell=2.0$
0.2	4.24×10^{-4}	6.28×10^{-4}	5.09×10^{-4}
0.4	1.70×10^{-3}	2.50×10^{-3}	2.02×10^{-3}
0.6	3.87×10^{-3}	5.56×10^{-3}	4.50×10^{-3}
0.8	1.86×10^{-2}	9.77×10^{-3}	7.88×10^{-3}

We now perform numerical calculations for the three values of ℓ above with incident angles $\theta=0$ and 30^o using the same discretization parameters as in Section 5.1. The magnitude of the mean energy defect $|\overline{e}|$ and the standard deviation σ_e for various ε are displayed in Tables 3 to 6 for $\theta=0,30^o$, respectively. Interestingly, we observe that when the incident angle is set to $\theta=0$, for fixed ε higher accuracy is obtained as the correlation length increases (the surface becomes smoother), however, when the incident angle is $\theta=30^o$, the same order of accuracy is observed for surfaces with all three different correlation lengths.

6 Conclusion

We presented an efficient numerical method based upon a combination of the Monte Carlo method and the transformed field expansion for the simulation of electromagnetic wave scattering by random rough surfaces. One compelling feature of the algorithm is that the governing equations for all samples at each perturbation order shares the common deterministic Helmholtz operator, hence all the solutions can be obtained in an efficient manner by simple forward and backward substitutions. One future direction is to extend the proposed method for electromagnetic scattering by two dimensional random rough surfaces, this would require solving the full Maxwell's equations over random domains. Another challenging problem is to develop numerical methods for wave scattering by non-periodic random rough surface.

Acknowledgments

The work of the first author was partially supported by the NSF grant DMS-1318486, the work of the second author was partially supported by the NSF grant DMS-1417676, and the work of the third author was partially supported by the NSF grant DMS-1522548. The second author also gratefully acknowledges the support and hospitality provided by the IMA in University of Minnesota during his visit and when part of this project is performed.

References

[1] G. Bao, D. Dobson, and J. Cox, Mathematical studies in rigorous grating theory, J. Opt. Soc. Am. A, 12 (1995), 1029-1042.
[2] G. Bao and P. Li, Near-field imaging of infinite rough surfaces, SIAM J. Appl. Math., 73 (2013): 2162-2187.
[3] I. Babuška, F. Nobile and R. Tempone, A stochastic collocation method for elliptic partial differential equations with random input data, SIAM Rev., 52 (2010), 317-355.
[4] I. Babuška, R. Tempone and G. E. Zouraris, Galerkin finite element approximations of stochastic elliptic partial differential equations, SIAM J. Numer. Anal., 42 (2004), 800-825.
[5] D. Berman and J. Perkins, The Kirchhoff approximation and first order perturbation theory for rough surface scattering, J. Acoust. Soc. Amer., 78 (1985), 1045-1051.
[6] R. Caflisch, Monte Carlo and quasi-Monte Carlo methods, Acta Numerica, 7 (1998), 1-49.
[7] C. Canuto and T. Kozubek, A fictitious domain approach to the numerical solution of PDEs in stochastic domains, Num. Math., 107 (2007), 257.
[8] J. Castrillon-Candas, F. Nobile, and R. Tempone, Analytic regularity and collocation approximation for elliptic PDEs with random domain deformations, Comput. Math. Appl., 71 (2016), 1173-1197.
[9] C. Chan, L. Tsang, and Q. Li, Monte Carlo simulations of large-scale one-dimensional random rough-surface scattering at near-grazing incidence: Penetrable case, IEEE Trans. Antenn. Propag., 46 (1998), 142-149.

[10] M. Deb, I. Babuška, and J. Oden, Solution of stochastic partial differential equations using Galerkin finite element techniques, Comput. Methods Appl. Mech. Engrg., 190 (2001), 6359-6372.
[11] X. Feng, J. Lin, and C. Lorton, An efficient numerical method for acoustic wave scattering in random media, SIAM/ASA J. Uncertainty Quantification, 3 (2015), 790-822.
[12] X. Feng, J. Lin, and C. Lorton, A multi-modes Monte Carlo finite element method for elliptic partial differential equations with random coefficients, Int. J. Uncertainty Quantification, 6 (2016), 429-443.
[13] A. Fung, Z. Li, and K. Chen, Backscattering from a randomly rough dielectric surface, IEEE Trans. Geo. Remote Sensing, 30 (1992), 356-369.
[14] N. Garcia and E. Stoll, Monte Carlo calculation for electromagnetic-wave scattering from random rough surfaces, Phy. Rev. Lett., 52 (1984), 1798.
[15] Y. He, D. P. Nicholls, and J. Shen, An efficient and stable spectral method for electromagnetic scattering from a layered periodic structure, J. Comput. Phy., 231 (2012), 3007-3022.
[16] B. Hu and D. P. Nicholls, Analyticity of Dirichlet-Neumann Operators on Hölder and Lipschitz Domains, SIAM J. Math. Anal., 37 (2005), 302–320.
[17] A. Ishimaru, *Wave Propagation and Scattering in Random Media* (IEEE Press, New York, 1997).
[18] J. Johnson, L. Tsang, R. Shin, K. Pak, C. Chan, A. Ishimaru, and Yasuo Kuga, Backscattering enhancement of electromagnetic waves from two-dimensional perfectly conducting random rough surfaces: A comparison of Monte Carlo simulations with experimental data, IEEE Trans. Antenn. Propog., 44 (1996), 748.
[19] P. Kowalczewski, M. Liscidini, and L. Andreani, Engineering Gaussian disorder at rough interfaces for light trapping in thin-film solar cells, Opt. Lett., 37 (2012), 4868-4870.
[20] G. Lord, C. Powell, and T. Shardlow, *An Introduction to Computational Stochastic PDEs*, (Cambridge University Press, 2014).
[21] A. Narayan and T. Zhou, Stochastic collocation methods on unstructured meshes, Commun. Comput. Phys., 18 (2015), pp. 1-36.
[22] D. P. Nicholls and F. Reitich, A new approach to analyticity of Dirichlet-Neumann operators, Proc. Roy. Soc. Edinburgh Sect. A, 131 (2001), 1411–1433.
[23] D. P. Nicholls, F. Reitich, T. W. Johnson, and S.-H. Oh, Fast high-order perturbation of surfaces (HOPS) methods for simulation of multi-layer plasmonic devices and metamaterials, J. Opt. Soc. Am. A, 31 (2014), 1820-1831.
[24] D. P. Nicholls and F. Reitich, Shape deformations in rough surface scattering: improved algorithms, J. Opt. Soc. Am. A, 21 (2004), 606-621.
[25] M. Nieto-Vesperinas and J. Soto-Crespo, Monte Carlo simulations for scattering of electromagnetic waves from perfectly conductive random rough surfaces, Opt. Lett., 12 (1987), 979-981.
[26] J. A. Ogilvy, *Theory of Wave Scattering from Random Rough Surfaces*, (AdamHilger, 1991).
[27] R. Petit (Ed.), *Electromagnetic Theory of Gratings*, (Springer-Verlag, Berlin, 1980).
[28] H. Raether, *Surface Plasmons on Smooth and Rough Surfaces and on Gratings*, (Springer-Verlag, Berlin, 2013).
[29] S. Rice, Reflection of electromagnetic waves from slightly rough surfaces, Commun. Pure Appl. Math., 4 (1951), 351-378.
[30] A. Shchegrov, A. Maradudin, and E. Méndez, Multiple scattering of light from randomly rough surfaces, Progress in Optics, 46 (2004), 117-241.
[31] J. Shen, T. Tang, and L.-L. Wang, *Spectral methods*, *Springer Series in Computational Mathematics*, 41 (Springer, Heidelberg, 2011).

[32] I. Simonsen, A. Maradudin, and T. Leskova, Scattering of electromagnetic waves from two-dimensional randomly rough perfectly conducting surfaces: The full angular intensity distribution, Phy. Rev. A, 81 (2010), 013806.
[33] K. Warnick and W. Chew, Numerical simulation methods for rough surface scattering, Waves in Random Media, 11 (2001), R1-R30.
[34] D. Xiu and J. Shen, An efficient spectral method for acoustic scattering from rough surfaces, Commun. Comput. Phys., 1 (2007), 54-72.
[35] D. Xiu and G. Karniadakis, Modeling uncertainty in steady state diffusion problems via generalized polynomial chaos, Comput. Methods Appl. Math. Engrg., 191 (2002), 4927-4948.
[36] D. Xiu and D. Tartakovsky, Numerical methods for differential equations in random domains, SIAM J. on Sci. Comput., 28 (2006), 1167-1185.